Available online at www.sciencedirect.com
ScienceDirect
Trans. Nonferrous Met. Soc. China 30(2020) 1615−1624
Transactions of Nonferrous Metals Society of China
www.tnmsc.cn

Boosting ethanol oxidation over nickel oxide through construction of quasi-one-dimensional morphology and hierarchically porous structure

Jing ZHAN[1,2], Ze-lin MIAO[1], Meng CAI[1], Qi-hou LI[1,2]

1. School of Metallurgy and Environment, Central South University, Changsha 410083, China;
2. National Engineering Laboratory for High Efficiency Recovery of Refractory Nonferrous Metals Resources, Changsha 410083, China

Received 9 August 2019; accepted 14 April 2020

Abstract: Quasi-one-dimensional NiO with a hierarchically porous structure was synthesized through a facile coordination−precipitation method with the coupling effect of ammonia and a post-calcination treatment. The electrocatalytic properties of NiO fibers for the oxidation of ethanol were compared with those of NiO spheres. The results show that the fibrous NiO possesses a larger specific surface area of 140.153 m^2/g and a lower electrical resistivity of 4.5×10^5 Ω·m, leading to an impressively superior electrocatalytic activity to spherical NiO for ethanol oxidation in alkaline media. The current decay on fibrous NiO at 0.6 V in 100−900 s was 0.00003%, which is much lower than that of spherical NiO, indicating its better stability. The unique morphology and hierarchically porous structure give the fibrous NiO great potential to be used as an anodic electrocatalyst for direct ethanol fuel cells.
Key words: hierarchically porous structure; nickel oxide; ethanol oxidation; quasi-one-dimensional morphology

1 Introduction

Direct ethanol fuel cells (DEFCs) have attracted considerable attention as one of the most promising energy storage and conversion devices in terms of their numerous advantages including high efficiency, moderate operating conditions and green emissions [1,2]. However, there still remains a big challenge to achieve the total oxidation of ethanol directly to carbon dioxide, which involves the cleavage of C—C bonds and the transfer of 12 electrons per molecule [3]. The development of anode catalysts with high performance and good stability is undoubtedly critical for the commercialization of DEFCs. Precious metals such as Pt, Pd and their alloys or composites have been intensively investigated due to their high electrocatalytic activity for ethanol/methanol oxidation [4−6]. Nevertheless, the drawbacks, including the high cost due to the scarce reserves and the poor durability resulting from self-poisoning by absorbing intermediates such as CO, impede their industrial production and daily application [7,8]. As a result, many alternative cost-efficient electrocatalysts such as non-precious transition metals, especially nickel-based materials, have been exploited for the direct electro-oxidation of alcohols [9−13].

Nickel oxide (NiO) is regarded as one of the most applicable catalytic materials because of its low cost, good durability, easy fabrication and acceptable electrochemical properties [14,15]. However, due to the high electronic resistance and

Foundation item: Project (51404306) supported by the National Natural Science Foundation of China; Project (JNJJ201613) supported by Jiana Foundation of Central South University, China; Project (2017YFC0210401) supported by the National Key Research and Development Program of China
Corresponding author: Jing ZHAN; Tel: +86-13975147556; E-mail: 80560381@qq.com;
Qi-hou LI; Tel: +86-13975158738; E-mail: li_qihou@126.com
DOI: 10.1016/S1003-6326(20)65324-9

low charge transfer rate, bulk NiO usually exhibits low electrocatalytic activity, which largely limits its application in alcohol oxidation. To solve this problem, apart from dispersing NiO particles in a conductive substrate, such as carbon materials, to form the composites [10], the conductivity and the electrocatalytic activity of NiO can also be effectively improved by endowing it with unique morphologies and structures. Generally, the construction of one-dimensional (1D) nano-structures such as nanowires [16], nanorods [17], and nanotubes [18] is beneficial to enhancing the performance of electrocatalysts due to the efficiently shortened mass transportation pathways and the increased conductivity [19]. Additionally, compared with dense materials, the porous structure could enlarge the specific surface area of catalysts and expose richer active sites, which tremendously benefits the interfacial contact between the electrode/electrolyte and improves the efficiency of the electrocatalysts [20,21]. Thus, the construction of a porous 1D structure would greatly ameliorate the aforementioned drawbacks of NiO particles, making it a great potential material to be used as the anodic electrocatalyst in DEFCs.

In our previous work [22−24], the synthesis conditions that affect the morphology of precursors and the final NiO products, as well as the related thermodynamic issues were systematically investigated. It was concluded that the introduction of ammonia is a key to shape the precursors into the fibrous morphology. In this work, we will mainly focuse on the electrocatalytic activity of the as-prepared fibrous NiO powders for ethanol oxidation according to the advantages of its unique morphology and structure. Meanwhile, the electrocatalytic activity and conductivity of the spherical NiO will be involved for comparison.

2 Experimental

2.1 Reagents and materials

Nickel chloride hexahydrate ($NiCl_2·6H_2O$), oxalic acid dihydrate ($H_2C_2O_4·2H_2O$), ammonium hydroxide ($NH_3·H_2O$), polyvinylpyrrolidone (PVP), sodium hydroxide (NaOH) and ethanol (C_2H_5OH) were purchased from Changsha Sublimation Scientific Research (Changsha, China). Nafion (0.5 wt.%) was purchased from Alfa Aesar Co. Ltd. All reagents are of analytical grade and used as received without further purification. All solutions were freshly prepared with deionized water.

2.2 Synthesis of materials

In a typical synthetic experiment, 7.564 g of $H_2C_2O_4·2H_2O$ (0.6 mol) and 0.500 g of PVP were completely dissolved in a mixed solvent of 50 mL ethanol and 50 mL deionized water, and followed by the addition of 100 mL $NiCl_2·6H_2O$ solution (0.5 mol) at a rate of 2 mL/min with the temperature maintained at 333 K in a water bath. The pH value was adjusted in the range of 6.0−9.0 by adding $NH_3·H_2O$ and the suspension was stirred continuously for 60 min after the feeding. The precipitate was washed with water and ethanol, respectively, and dried under vacuum at 373 K for 24 h. Finally, the precipitate was annealed at 723 K in air for 1 h to obtain the NiO fibers (NiO-f).

The spherical NiO (NiO-s) for comparison was synthesized through the hydrothermal method using urea according to the literature method [25,26].

2.3 Characterization

The morphology of the as-prepared samples was observed via field-emission scanning electron microscopy (FESEM, Tescan MIRA3), transmission electron microscopy (TEM, FEI Tecnai G2 F20) and high-resolution transmission electron microscopy (HRTEM, FEI Tecnai G2 F20). An X-ray powder diffractometer (Rigaku-TTRIII) (Cu K_α, λ=0.154056 nm) was used to determine the phase structure and the composition of the precursors and final products. The resistivity of samples was measured using a four-point probe tester (RTS−8). The specific surface areas and average pore sizes were determined via N_2 adsorption/desorption analysis (Quadrasorb SI, Quantachrome). The Brunauer−Emmett−Teller (BET) specific surface areas were calculated from the adsorption isotherms, and the Barrett−Joyner−Halenda (BJH) pore size distribution was analyzed with the adsorption branch data.

2.4 Preparation of modified electrode

To make the electrocatalyst ink, 50 mg of as-prepared porous NiO fibers were ultrasonically dispersed into 2 mL deionized water. Then, 4 μL of the ink was transferred onto the surface of a pre-polished glassy carbon electrode (GCE, 5 mm in diameter) using pipette. After the solvent was

evaporated at the room temperature, the fibrous NiO was covered by 2 μL of Nafion solution (0.5 wt.%) to obtain the modified glassy carbon electrode (NiO-f/GCE). A spherical NiO modified glassy carbon electrode (NiO-s/GCE) was also prepared through the same method. The mass loading of each electrode is about 0.51 mg/m^2.

2.5 Electrochemical measurement

The electrocatalytic performance of the as-prepared samples for ethanol oxidation was evaluated with an electrochemical workstation (CHI660B) using a conventional three-electrode setup where the modified glassy carbon electrodes (NiO-f/GCE and NiO-s/GCE) were used as the working electrodes, while a saturated calomel electrode (SCE) and a Pt plate electrode were selected as the reference and counter electrodes, respectively. All of the electrochemical tests were performed at (25±2) °C.

3 Result and discussion

3.1 Preparation and physical characterization of NiO fibers and spheres

Figure 1 shows the FESEM images of the NiO precursors obtained by coordination−precipitation method at different pH values. When the pH is adjusted to 6.0 by adding $NH_3{\cdot}H_2O$, an aggregated granular morphology is observed (Fig. 1(a)). Then, the precursors transfer into flower-like particles accumulated by numerous nanorods when pH=7.0 (Fig. 1(b)). With the further increase of the pH value (pH>8.0), the precursors display a fibrous morphology with the diameter of 0.1−0.3 μm and an aspect ratio of 20−30 (Figs. 1(c, d)). However, the aspect ratio of the fibers decreases when the pH reaches 9.0, which may result from the dissolution of the precipitate due to the high concentration of ammonia in the suspension. These results indicate that the change of pH values due to the addition of $NH_3{\cdot}H_2O$ may have a significant effect on the morphology of the precursors.

According to the thermodynamics analysis [24], Ni(II) ions mainly exist as the form of $Ni[NH_3]_n^{2+}$ (n=1−6) at pH>7.0, and the complexing ion $Ni[NH_3]_m^{2+}$ (m=3−6) dominates only when pH≥8.0. Thus, for the reaction system of Ni(II)−$C_2O_4^{2-}$−NH_3−NH_4^+−H_2O, different coordination numbers of ammonia in $Ni[NH_3]_n^{2+}$ (n=1−6) may affect nickel oxalate species precipitated from the system, further influencing their morphologies. At certain pH values (8.0−8.4 for example), the quasi-one-dimensional precursors will be formed with the composition of nickel oxalate containing ammonia [22].

The NiO fibers were obtained through the post-calcination treatment of the fibrous nickel oxalate precursor precipitated at pH=8.0. Figure 2 shows the XRD patterns of the as-prepared NiO

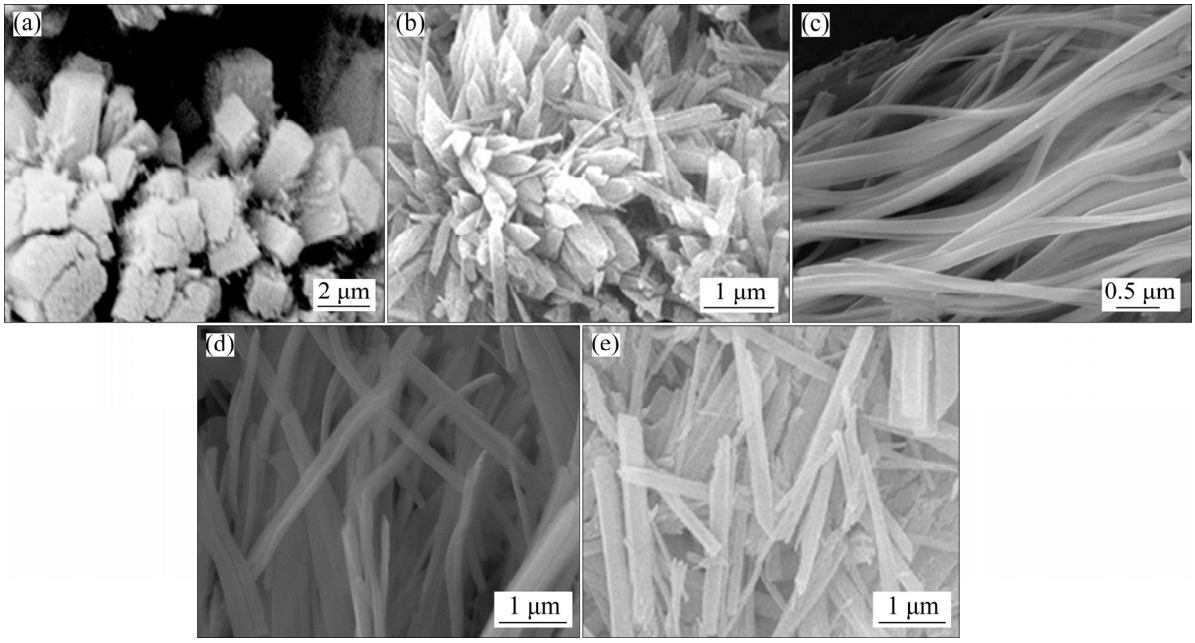

Fig. 1 FESEM images of NiO precursors obtained at different pH values of 6.0 (a), 7.0 (b), 8.0 (c), 8.4 (d) and 9.0 (e)

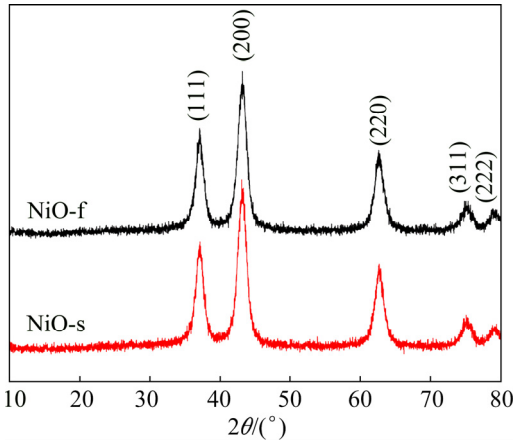

Fig. 2 XRD patterns of NiO fibers and NiO spheres

fibers and the spherical NiO for comparison. The diffraction peaks of the fibrous NiO correspond perfectly to facets indexed to the pure phase of face-centered cubic (fcc) NiO (JCPDS No. 73-1523). No other diffraction peaks are observed. Similarly, the XRD patterns of NiO spheres can also be assigned to the NiO phase without impurities detected.

The FESEM images of the NiO fibers are presented in Fig. 3(a). It is shown that the prepared NiO powders are in a well-dispersed fibrous morphology with an average diameter of 200 nm where numerous pores distribute uniformly throughout the whole fibers, which can be ascribed to the release of NH_3 and CO_2 during the calcination process. The porous structure is also confirmed by the TEM image (Fig. 3(b)) which shows that the NiO fibers are constructed by many interconnected nanoparticles at the length scale of 10−20 nm. Meanwhile, it can be observed in HRTEM image (Fig. 3(c)) that the distance between the adjacent discerned lattice fringes is 0.241 nm, which can be indexed to the (111) crystal plane of NiO. Moreover, the SAED pattern (inset of Fig. 3(c)) exhibits well-defined diffraction rings, suggesting polycrystalline characteristic of NiO fibers. These rings can be indexed to the (111), (200), (220), (311), (222) planes of the NiO phase, which matches well with the above XRD results. For comparison, the morphology of the NiO-s sample was also observed (Fig. 3(d)), exhibiting aggregated irregular spheres with an average diameter of 1 μm and no distinct pores. It is expected that porous structure of NiO fibers obtained by the coordination−precipitation and post-calcination method could greatly boost the transportation of ions and electrons both at and beneath the electrolyte/electrode interface, which would facilitate the electro-oxidation of ethanol on the NiO modified electrode.

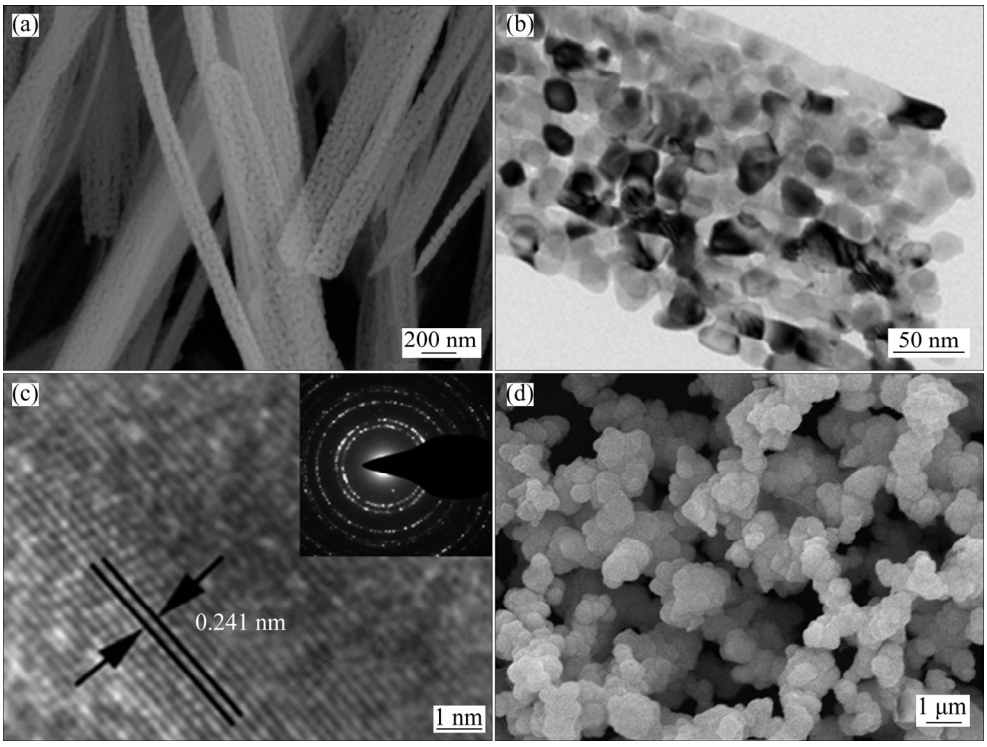

Fig. 3 FESEM image (a), TEM image (b) and HRTEM image (inset: SAED pattern) (c) of prepared NiO-f sample, and FESEM image of NiO-s sample (d)

The suggested one-dimensional growth mechanism of fibrous NiO precursor and the formation of the porous structure on the final NiO powders are illustrated in Fig. 4. Here, we put forward that the coordination of ammonia into nickel oxalate is the key factor, and the aggregation of thousands of tiny crystals gives rise to the orientated growth of precursors due to the different energies of the crystal surfaces, which is similar to the precipitation reactions of other oxalate salts [27,28]. During the calcination process, through the release of volatile gases such as NH_3 and CO_2, the NiO fibers display a unique porous structure, as shown by the FESEM and TEM images.

To further confirm the existence of the pores, N_2 isotherms and pore size distributions of as-prepared NiO fibers are depicted in Fig. 5. According to the International Union of Pure and Applied Chemistry (IUPAC) classification [29], the isotherms of NiO fibers can be classified as Type IV with H_3 hysteresis loop corresponding to the feature of mesoporous structure, indicating more active catalytic sites existing in NiO particles for the direct electro-oxidation of ethanol. The steep rise of the isotherms when P/P_0 approaches 1 indicates the presence of macropores in fibrous NiO powders, which allows for the efficient transportation of reactants and by-products at the interface of the electrode and electrolyte. The specific surface area of the sample is calculated to be 140.153 m^2/g, which is much larger than that of the spherical NiO (35.305 m^2/g) and NiO reported in other studies [30−32]. As shown in Fig. 5(b), the pore diameter of the NiO fibers mainly distributes around 3.34 and 23.67 nm where the former is dominant. The average pore diameter and the pore

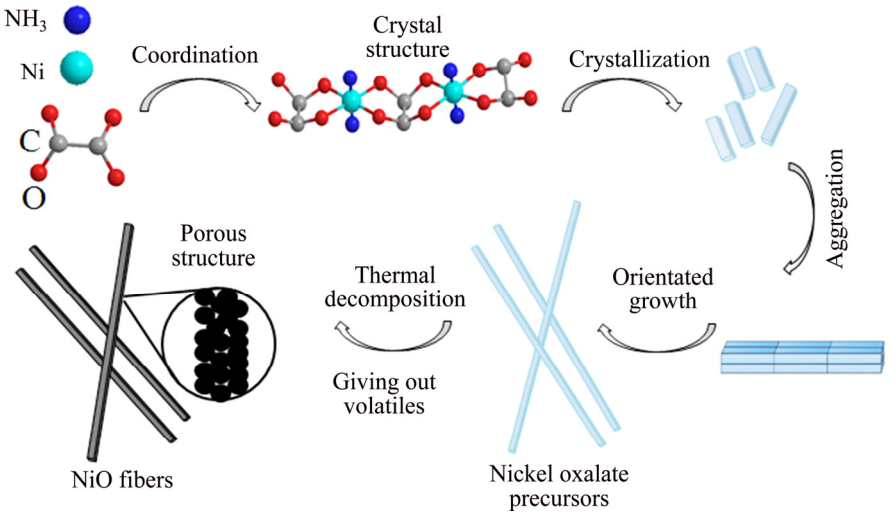

Fig. 4 Schematic illustration of growth mechanism of fibrous precursors and formation of porous structure on NiO powders

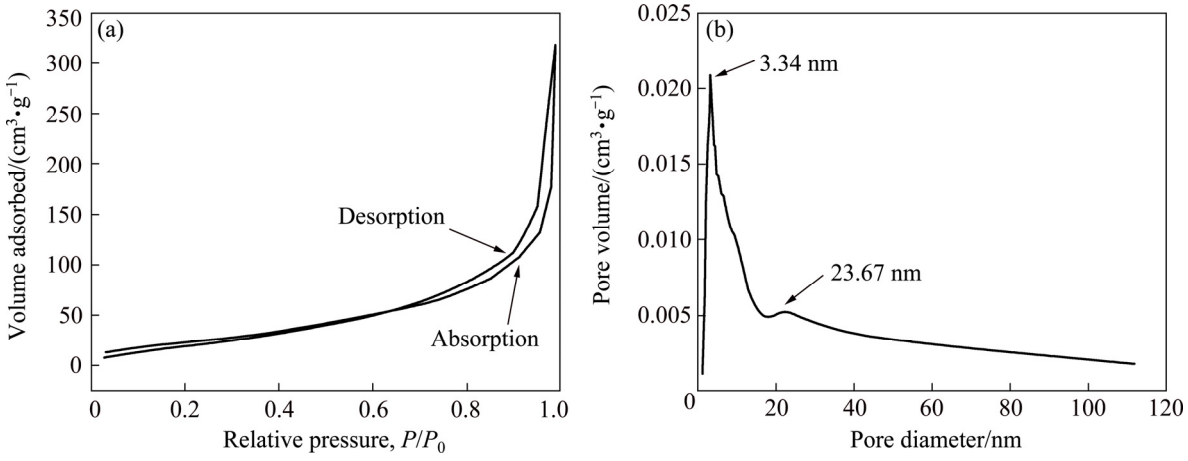

Fig. 5 N_2 sorption isotherms (a) and pore-size distribution (b) of NiO fibers

volume are 3.343 nm and 0.00521 cm^3/g, respectively. Furthermore, the electrical conductivity measurement of the NiO samples was conducted using a four-point probe tester. Impressively, the resistivity of NiO fibers is measured to be 4.5×10^5 Ω·m (corresponding to the conductivity of 2.2×10^{-6} S/m), which is one order of magnitude lower than that of NiO spheres of 3.6×10^6 Ω·m (corresponding to the conductivity of 2.7×10^{-7} S/m). This might be due to the one-dimensional and porous structure which could effectively lower the percolation threshold [19,33] and enhance the electrical conductivity of NiO by offering a network built with the conductive loops.

3.2 Electrocatalytic properties of NiO fibers and spheres

Figure 6(a) shows the cyclic voltammograms (CVs) of the NiO fiber modified glassy carbon electrode (NiO-f/GCE) in 1 mol/L NaOH in the absence and presence of 0.1 mol/L ethanol recorded at a scan rate of 10 mV/s. A pair of redox peaks at 0.36 and 0.47 V exist in the absence of ethanol, which can be ascribed to the transformation between Ni^{2+} and Ni^{3+} [9,34]. When 0.1 mol/L ethanol is added, a significantly increased anodic peak current is observed at about 0.58 V, indicating the involvement of ethanol in the electrochemical reaction on the surface of NiO-f/GCE. For comparison, CVs of the spherical NiO modified glassy carbon electrode (NiO-s/GCE) in 1 mol/L NaOH in the absence and presence of 0.1 mol/L ethanol are also shown in Fig. 6(b). Similarly, an increased anodic current is observed in the presence of ethanol. However, the current increment is much smaller than that of NiO-f/GCE, indicating its inferior electrocatalytic activity for the electro-oxidation of ethanol.

The following mechanism is put forward for the ethanol oxidation on NiO/GCE. First, a layer of $Ni(OH)_2$ forms rapidly in NaOH solution at low potentials during the anodic sweeping. At a certain higher potential, the redox reaction of Ni^{2+}/Ni^{3+} occurs according to Eq. (1) [35,36]. Then, ethanol is oxidized on the electrode surface via Eq. (2) [37]:

$$Ni(OH)_2+OH^- \rightleftharpoons NiOOH+H_2O+e \quad (1)$$

$$NiOOH+ethanol \rightleftharpoons Ni(OH)_2+product \quad (2)$$

The CV curves of NiO-f/GCE and NiO-s/GCE in the presence of 0.1 mol/L ethanol in 1 mol/L NaOH solution are shown in Fig. 6(c) for further comparison. It can be seen that the CV curve of NiO-f/GCE shows a larger enclosed area, representing a higher current density for ethanol oxidation than that of NiO-s/GCE. In addition, the onset potential for the ethanol oxidation reaction on NiO-f/GCE is lower than that of NiO-s/GCE. Both

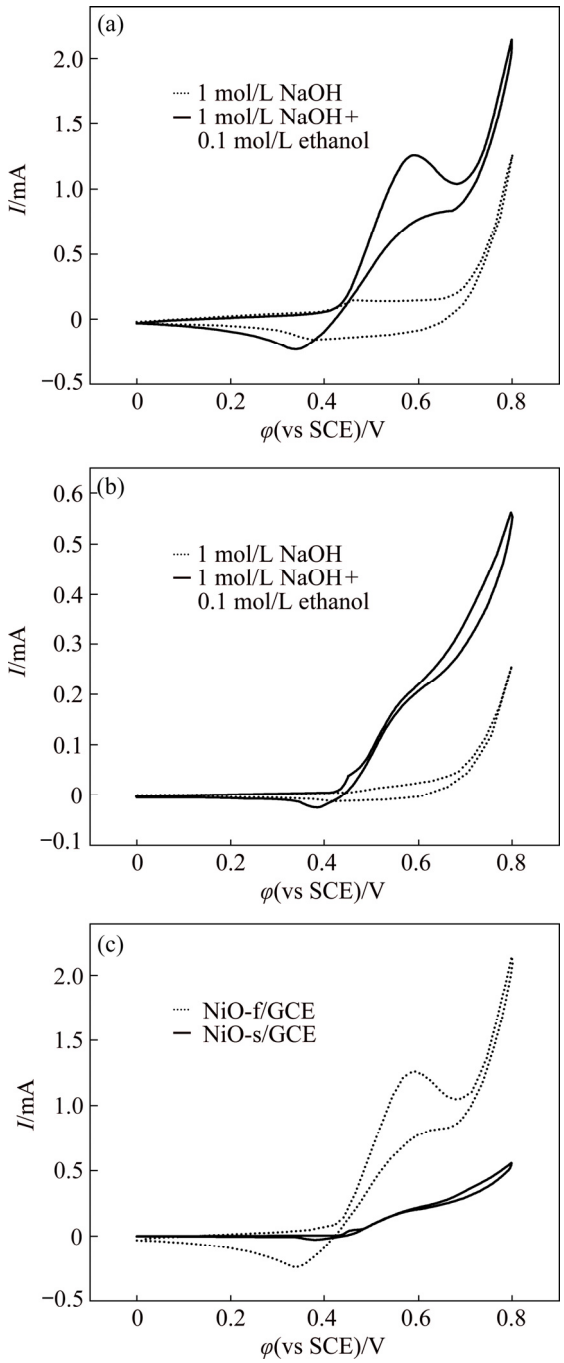

Fig. 6 CVs of NiO-f/GCE (a) and NiO-s/GCE (b), and comparison between NiO-f/GCE and NiO-s/GCE (c) in 1 mol/L NaOH in absence and presence of 0.1 mol/L ethanol (scan rate: 10 mV/s)

of them indicate the superior electrocatalytic activity of NiO-f/GCE to NiO-s/GCE, implying that the larger surface area and the better electrical conductivity derived from the quasi-one-dimensional morphology and hierarchical porous structure of NiO fibers are beneficial for the electrocatalytic oxidation of ethanol in alkaline media.

To further investigate the electrocatalytic performance of NiO-f/GCE, the effects of both ethanol concentration and scan rate were investigated by CV measurement. The CVs of NiO-f/GCE in 1 mol/L NaOH solution varying with increasing concentrations of ethanol are shown in Fig. 7(a). It can be observed that the anodic peak currents in the voltage range of 0.4−0.6 V vary linearly with the concentration of ethanol in the electrolyte (the inset image of Fig. 7(a)). Furthermore, the CVs of NiO-f/GCE at different scan rates with the electrolyte mixture of 0.1 mol/L ethanol and 1 mol/L NaOH are shown in Fig. 7(b). As observed, the peak current gradually increases as the scan rate varies from 10 to 50 mV/s. The inset image of Fig. 7(b) shows that the anodic peak currents are linearly proportional to the square root of the scan rates as well, implying that the kinetics of the ethanol electro-oxidation reaction on NiO-f/GCE is controlled by the diffusion of ethanol from the electrolyte to the electrode/electrolyte interface.

The current−time (I−t) curves of NiO-f/GCE and NiO-s/GCE were measured to compare their stability. As shown in Fig. 8(a), the current on NiO-f/GCE decreases rapidly during the first 100 s, which might be due to the adsorption of intermediates such as CO or CHO on the active

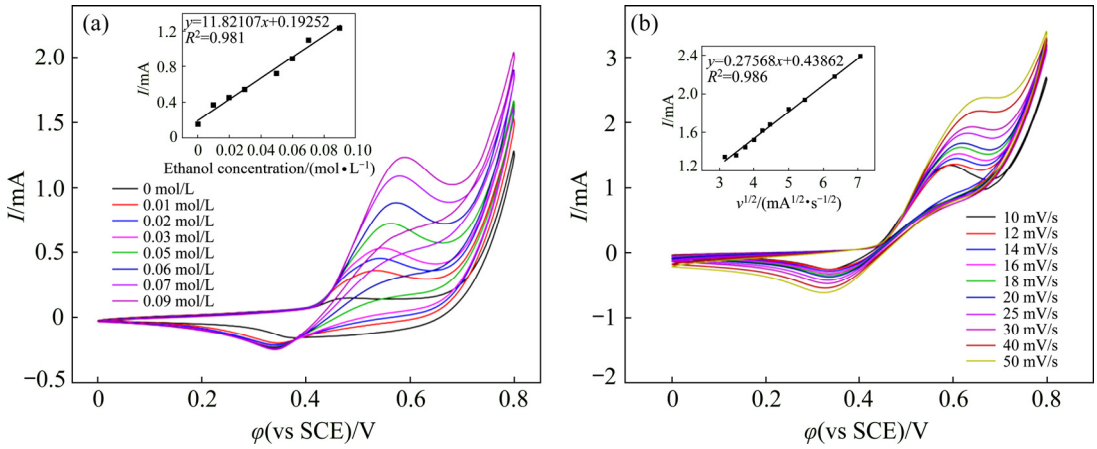

Fig. 7 CVs of NiO-f/GCE in 1 mol/L NaOH solution: (a) In presence of ethanol with various concentrations at scan rate of 10 mV/s (inset: dependency of anodic peak current on concentration of ethanol in 1 mol/L NaOH solution); (b) In presence of 0.1 mol/L ethanol at different scan rates (inset: dependency of anodic peak current on square root of scan rate)

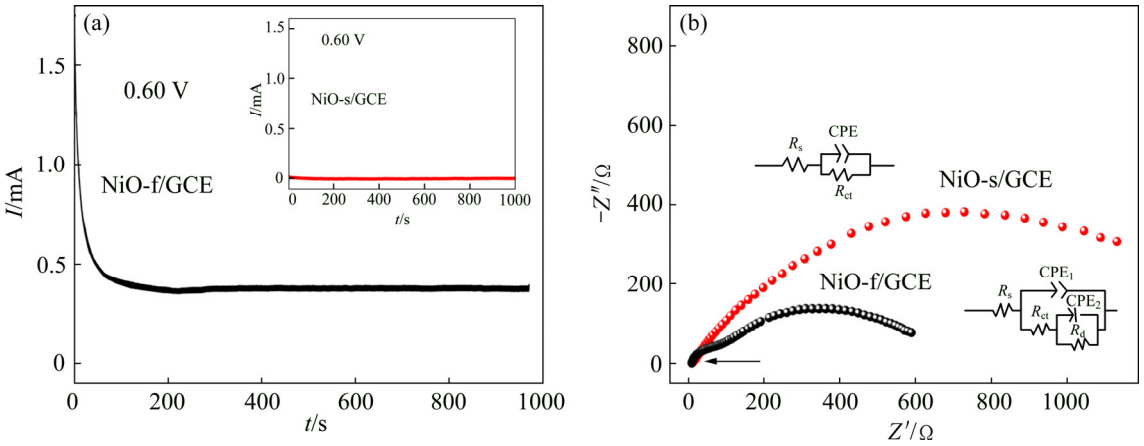

Fig. 8 I−t curves of NiO-f/GCE and NiO-s/GCE [26] (inset) (a) and Nyquist diagram of NiO-f/GCE and NiO-s/GCE (inset: corresponding equivalent circuit) (b) in presence of 0.1 mol/L ethanol in 1 mol/L NaOH solution

catalytic sites during the ethanol oxidation process. Shortly afterwards, the current stabilizes at a limiting value in the subsequent time range. Similar behavior of the current is observed for NiO-s/GCE (inset). However, the result of NiO-f/GCE shows a significantly larger current within the whole test time range, which further confirms the superior electrocatalytic activity of NiO fibers. In addition, almost no current decay (0.00003% in 100−900 s) is observed from the *I*−*t* curves of NiO-f/GCE, while the current decay on NiO-s/GCE is about 0.075% [26], implying the better stability of NiO fibers than the NiO spheres.

Furthermore, the electrochemical impedance spectroscopy (EIS) was applied to investigating the charge transfer behavior of NiO-f/GCE and NiO-s/GCE. As shown in Fig. 8(b), a depressed semicircle is observed from the results of NiO-s/GCE, which is related to both the charge transfer resistance and the double layer capacitance. NiO-f/GCE demonstrates a different diagram composed of a small semicircle at the high frequency region (arrow-pointed area) and a larger one within the middle−low frequency region. Similarly, the depressed semicircle at the high-frequency region corresponds to the combination of charge transfer resistance and the double layer capacitance due to the blocking effect of the rough electrode surface. The larger semicircle at the middle−low frequency region is ascribed to the diffusion impedance. It can be clearly seen that the diameter of the first semicircle for NiO-f/GCE is much smaller than that of the semicircle of NiO-s/GCE, indicating its lower charge transfer resistance. To further investigate the kinetics of ethanol oxidation on NiO-f/GCE, an equivalent circuit compatible with the EIS results is presented in Fig. 8(b). In the circuit, R_s, R_{ct} and R_d represent the solution resistance, charge transfer resistance and diffusion resistance, respectively. The CPE_1 and CPE_2 are the constant phase elements corresponding to the double-layer capacitance. The R_s and R_{ct} values obtained by fitting the experimental data are 7.981 and 77.17 Ω, respectively. Similarly, the R_s (9.29 Ω) and R_{ct} (156.6 Ω) for NiO-s/GCE are also obtained (inset in Fig. 8(b)). The similar fitting solution resistance (R_s) for these two electrodes indicates their identical electrolyte conditions, while the R_{ct} value of NiO-f/GCE is only about half that of NiO-s/GCE, implying the faster charge transfer characteristics of fibrous NiO than spherical NiO, which reconfirms the boosting effect for electro-oxidation of ethanol through the construction of quasi-one-dimensional and hierarchically porous structure in NiO powders.

4 Conclusions

(1) The NiO fibers can be synthesized through a facile template-free method, which involves the precipitation of the ammonia-containing nickel oxalate precursor and the post-calcination treatment. The introduction of ammonia plays the key role in obtaining the quasi-one-dimensional morphology and hierarchically porous structure of NiO samples.

(2) The synthesized NiO fibers has a higher specific surface area of 140.153 m^2/g and a lower resistivity of 4.5×10^5 Ω·m than NiO spheres, which are beneficial to enriching the active catalytic sites and the diffusion and transportation of ions and electrons.

(3) Profiting from the unique quasi-one-dimensional porous structure, the NiO fibers exhibit higher electrocatalytic activity and better stability than NiO spheres for electro-oxidation of ethanol in alkaline media, making it a promising anodic catalyst material for the high-performance DEFCs.

References

[1] CAI Qian, HONG Wen-ting, LI Jing, JIAN Chuan-yong, LIU Wei. A silicon photoanode for efficient ethanol oxidation under alkaline conditions [J]. RSC Advances, 2017, 7: 21809−21814.

[2] ZHANG Gen-lei, YANG Zhen-zhen, ZHANG Wen, HU Hong-wei, WANG Chun-zhen, HUANG Cheng-de, WANG Yu-xin. Tailoring the morphology of Pt_3Cu_1 supported on graphene nanoplates for ethanol oxidation [J]. Nanoscale, 2016, 8: 3075−3084.

[3] ZHAI Chun-yang, HU Jia-yue, SUN Ming-juan, ZHU Ming-shan. Two dimensional visible-light-active Pt-BiOI photoelectrocatalyst for efficient ethanol oxidation reaction in alkaline media [J]. Applied Surface Science, 2018, 430: 578−584.

[4] SARKAR S, JANA R, VADlAMANI H, RAMANI S, MUMBARADDI D, PETER S C. Facile aqueous-phase synthesis of the $PtAu/Bi_2O_3$ hybrid catalyst for efficient electro-oxidation of ethanol [J]. ACS Applied Materials and Interfaces, 2017, 9: 15373−15382.

[5] LIU Xin-yi, WANG Ying-min, QIANG Jian-bing, WANG Bao-lin, MA Dian-guo, ZHANG Wei, DONG Chuang. Preperation and electro-catalytic activity of nanoporous palladium by dealloying rapidly-quenched $Al_{70}Pd_{17}Fe_{13}$ quasicrystalline alloy [J]. Transactions of Nonferrous Metals

Society of China, 2019, 29: 785−790.

[6] LI Zhi-juan, CHEN Yi-fan, FU Geng-tao, CHEN Yang, SUN Dong-mei, LEE J, TANG Ya-wen. Porous PdRh nanobowls: Facile synthesis and activity for alkaline ethanol oxidation [J]. Nanoscale, 2019, 11: 2974−2980.

[7] FETOHI A E, AMIN R S, HAMEED R M A, EL-KHATIB K M. Effect of nickel loading in Ni@Pt/C electrocatalysts on their activity for ethanol oxidation in alkaline medium [J]. Electrochimica Acta, 2017, 242: 187−201.

[8] FARSADROOH M, NOROOZIFAR M, MODARRESI-ALAM A R, SARAVANI H. Sonochemical synthesis of high-performance Pd@CuNWs/MWCNTs-CH electrocatalyst by galvanic replacement toward ethanol oxidation in alkaline media [J]. Ultrasonics Sonochemistry, 2019, 51: 478−486.

[9] SOLIMAN A B, ABDEL-SAMAD H S, ABDEL RHHIM S S, AHMED M A, HASSAN H H. High performance nano-Ni/Graphite electrode for electro-oxidation in direct alkaline ethanol fuel cells [J]. Journal of Power Sources, 2016, 325: 653−663.

[10] TONG Xi-li, QIN Yong, GUO Xiang-yun, MOUTANABBIR O, AO Xian-yu, PIPPEL E, ZHANG Lian-bing, KNEZ M. Enhanced catalytic activity for methanol electro-oxidation of uniformly dispersed nickel oxide nanoparticles—Carbon nanotube hybrid materials [J]. Small, 2012, 8: 3390−3395.

[11] LONG Yi-yu, ZHAN Jing, HUANG Jian-yang. Porous nickel fibers with enhanced electrocatalytic activities on electro-oxidation of ethanol in alkaline media [J]. Journal of the Minerals, Metals and Materials Society, 2019, 71: 1485−1491.

[12] JAYASEELAN S S, KO T, RADHAKRISHNAN S, YANG C, KIM H, KIM B. Novel MWCNT interconnected $NiCo_2O_4$ aerogels prepared by a supercritical CO_2 drying method for ethanol electrooxidation in alkaline media [J]. International Journal of Hydrogen Energy, 2016, 41: 13504−13512.

[13] ZHAN Jing, CAI Meng, ZHANG Chuan-fu, WANG Chen. Synthesis of mesoporous $NiCo_2O_4$ fibers and their electrocatalytic activity on direct oxidation of ethanol in alkaline media [J]. Electrochimica Acta, 2015, 154: 70−76.

[14] ZHAN Si-hui, ZHOU Zhi-ruo, LIU Man-man, JIAO Yong-li, WANG Hai-tao. 3D NiO nanowalls grown on Ni foam for highly efficient electro-oxidation of urea [J]. Catalysis Today, 2019, 327: 398−404.

[15] MORAES M C, JUNCO G G, MOREIRA T F M, PINHEIRO C J G, OLIVI P, PROFETI D. NiO-promoted Pt electrocatalysts prepared by thermal decomposition of polymeric precursors for oxidation of glycerol in alkaline medium [J]. Journal of Environmental Chemical Engineering, 2019, 7: 102922.

[16] LIU Kai, WANG Wei, GUO Peng-hui, YE Jing-yu, WANG Yuan-yuan, LI Ping-ting, LYU Zi-xi, GENG Yong-sheng, LIU Mao-chang, XIE Shui-fen. Replicating the defect structures on ultrathin Rh nanowires with Pt to achieve superior electrocatalytic activity toward ethanol oxidation [J]. Advanced Functional Materials, 2019, 29: 1806300.

[17] DU Xiao-qiang, SHAO Qi-zhao, ZHANG Xiao-shuang. Metal tungstate dominated $NiCo_2O_4$@$NiWO_4$ nanorods arrays as an efficient electrocatalyst for water splitting [J]. International Journal of Hydrogen Energy, 2019, 44: 2883−2888.

[18] YANG Guo-hai, ZHOU Ya-zhou, PAN Horng-bin, ZHU Cheng-zhou, FU Shao-fang, WAI C M, DU Dan, ZHU Jun-jie, LIN Yue-he. Ultrasonic-assisted synthesis of Pd−Pt/carbon nanotubes nanocomposites for enhanced electro-oxidation of ethanol and methanol in alkaline medium [J]. Ultrasonic Sonochemistry, 2016, 28: 192−198.

[19] GONG Shu, CHENG Wen-long. One-dimensional nanomaterials for soft electronics [J]. Advanced Electronic Materials, 2017, 3: 1600314.

[20] XU Chang-fan, ZHANG Kai-wen, ZHANG Da, CHANG Shi-lei, LIANG Feng, YAN Peng-fei, YAO Yao-chun, QU Tao, ZHAN Jing, MA Wen-hui, YANG Bing, DAI Yong-nian, SUN Xue-liang. Reversible hybrid sodium−CO_2 batteries with low charging voltage and long-life [J]. Nano Energy, 2020, 68: 104318.

[21] SONG Yan-yan, DUAN Dong, SHI Wen-yu, WANG Hai-yang, SUN Zhan-bo. Facile synthesis of 3D nanoporous Pd/Co_2O_3 composites with enhanced catalytic performance for methanol oxidation [J]. Transactions of Nonferrous Metals Society of China, 2018, 28: 676−686.

[22] ZHANG Chuan-fu, ZHAN Jing, WU Jian-hui, GUO Xue-yi, OKMIDO M. Preparation of fibrous nickel oxide particles [J]. Transactions of Nonferrous Metals Society of China, 2003, 13: 1440−1445.

[23] ZHANG Chuan-fu, ZHAN Jing, WU Jian-hui, LI Chang-jun. Preparation and characterization of fibrous NiO particles by thermal decomposition of nickelous complex precursors [J]. Transactions of Nonferrous Metals Society of China, 2004, 14: 713−717.

[24] ZHAN Jing, ZHANG Chuan-fu, LI Tie-jing, WU Jian-hui. Thermodynamic analysis on preparation of fibrous NiO precursor powders with oxalate precipitation process [J]. Transactions of Nonferrous Metals Society of China, 2005, 15: 926−930.

[25] ANU PRATHAP M U, SRIVASTAVA S. Synthesis of $NiCo_2O_4$ and its application in the electrocatalytic oxidation of methanol [J]. Nano Energy, 2013, 2: 1046−1053.

[26] ZHAN Jing, LU Er-ju, CAI Meng, MA Ya-lin. Electrocatalytic performance of spherical NiO for ethanol oxadation [J]. Chinese Journal of Engineering, 2016, 38: 1139−1144.

[27] OKAMOTO T, ICHINO R, OKIDO M, LIU Zhi-hong, ZHANG Chuan-fu. Effect of ammonia on the crystal morphology of nickel oxalate precipitates and their thermal decomposition into metallic nickel [J]. Materials Transactions, 2005, 46: 171−174.

[28] ZHANG Chuan-fu, YAO Yong-lin, ZHAN Jing, WU Jian-hui, LI Chang-jun. Template-free synthesis of Ni microfibres and their electromagnetic wave absorbing properties [J]. Journal of Physics D: Applied Physics, 2013, 46: 495308.

[29] SING K S W, EVERET D H, HAUL R A W, MOSCOU L, PIEROTTI R A, ROUQUÉROL J, SIEMIENIEWSKA T. Reporting physisorption data for gas/solid systems with special reference to the determination of surface area and porosity [J]. Pure and Applied Chemistry, 1985, 57: 603−619.

[30] ZHANG Xiao-jun, SHI Wen-hui, ZHU Ji-xin, ZHAO Wei-yun, MA Jan, MHAISALKAR S, MARIA T L, YANG Yan-hui, ZHANG Hua, HNG H H, YAN Qing-yu. Synthesis

of porous NiO nanocrystals with controllable surface area and their application as supercapacitor electrodes [J]. Nano Research, 2010, 3: 643−652.

[31] YANG Hong-zhi, ZOU Jian-peng. Controllable preparation of hierarchical NiO hollow microspheres with high pseudo-capacitance [J]. Transactions of Nonferrous Metals Society of China, 2018, 28: 1808-1818.

[32] GUND G S, LOKHANDE C D, PARK H S. Controlled synthesis of hierarchical nanoflake structure of NiO thin film for supercapacitor application [J]. Journal of Alloys and Compounds, 2018, 741: 549−556.

[33] AYATOLLAHI M R, SHADLOU S, SHOKRIEH M M, CHITSAZZADEH M. Effect of multi-walled carbon nanotube aspect ratio on mechanical and electrical properties of epoxy-based nanocomposites [J]. Polymer Testing, 2011, 30: 548−556.

[34] AL-ENIZI A M, GHANEM M A, EL-ZATAHRY A A, AL-DEYAB S S. Nickel oxide/nitrogen doped carbon nanofibers catalyst for methanol oxidation in alkaline media [J]. Electrochimica Acta, 2014, 137: 774−780.

[35] FLEISCHMANN M, KORINEK K, PLETCHER D. The oxidation of organic compounds at a nickel anode in alkaline solution [J]. Jouanal of Electroanalytical Chemistry and Interfacial Electrochemistry, 1971, 31: 39−49.

[36] PIETA I S, RATHI A, PIETA P, NOWAKOWSKI R, HOLDYNSKI M, PISAREK M, KAMINSKA A, GAWANDE M B, ZBORIL R. Electrocatalytic methanol oxidation over Cu, Ni and bimetallic Cu−Ni nanoparticles supported on graphitic carbon nitride [J]. Applied Catalysis B: Environmental, 2019, 244: 272−283.

[37] XU Chang-wei, HU Yong-hong, RONG Jian-hua, JIANG San-ping, LIU Ying-liang. Ni hollow spheres as catalysts for methanol and ethanol electrooxidation [J]. Electrochemistry Communications, 2007, 9: 2009−2012.

构筑准一维分级多孔结构对氧化镍电催化乙醇氧化的增强效应

湛 菁[1,2]，苗泽林[1]，蔡 梦[1]，李启厚[1,2]

1. 中南大学 冶金与环境学院，长沙 410083；
2. 难冶有色金属资源高效利用国家工程实验室，长沙 410083

摘 要：利用氨的配合作用，采用配位沉淀法及后续煅烧处理制备具有分级多孔结构的准一维 NiO 粉末。通过与球形 NiO 比较，对纤维状 NiO 催化乙醇氧化的电催化性能进行研究。结果表明，纤维状 NiO 具有更大的比表面积(140.153 m^2/g)以及更低的电阻率(4.5×10^5 Ω·m)，从而在碱性介质中对乙醇氧化反应具有更优越的电催化活性。在 0.6 V 极化电位下， 纤维状 NiO 在 100~900 s 的电流衰减仅为 0.00003%， 远低于球形 NiO，显示其更好的稳定性。这种特殊的形貌和分级多孔结构使纤维状 NiO 作为直接乙醇燃料电池的阳极电催化剂具有很大的应用潜力。

关键词：分级多孔结构；氧化镍；乙醇氧化；准一维形貌

(Edited by Bing YANG)